Available online at www.sciencedirect.com
SCIENCE DIRECT®
Journal of Sound and Vibration 293 (2006) 449–461
JOURNAL OF SOUND AND VIBRATION
www.elsevier.com/locate/jsvi

Short Communication

Limits of performance of mechanical band-pass filters used in energy scavenging

S.M. Shahruz*

Berkeley Engineering Research Institute, P.O. Box 9984, Berkeley, CA 94709, USA

Received 12 September 2005; received in revised form 27 September 2005; accepted 29 September 2005
Available online 5 December 2005

Abstract

In this note, the performance of mechanical band-pass filters to be used in energy scavengers is studied. Such a filter consists of an ensemble of cantilever beams where at the tip of each beam a mass, known as the proof mass, is mounted. Two questions are raised regarding the performance of the filter: (i) What is the best possible performance of the filter? (ii) How can a filter with such a performance be designed? In answering these questions, the limits of performance of the filter are determined. Knowledge of such limits leads to a systematic procedure for determining dimensions of the beams and masses of the proof masses of high-performance band-pass filters.

1. Introduction

The concept and practice of energy scavenging from the environment have been receiving much attention in recent years. An example of energy scavenging is the conversion of the energy of vibration sources, which is usually neglected, into usable but small electricity to power micro-electronic devices; see, e.g., Refs. [1–9]. Examples of vibration sources, the energy of which to be scavenged, are buildings, bridges, cars, trains, aircraft, ships, manufacturing tools, etc.

A device that scavenges energy efficiently from the environment is called an energy scavenger. A typical energy scavenger consists of a cantilever beam on which a piezoelectric film and a mass are mounted; see Fig. 1. This device will be referred to as either the energy scavenger or the beam–mass system. The mass on the cantilever beam is known as the proof mass. When the scavenger is mounted on a vibration source, say a panel, the cantilever beam would vibrate. The vibration of the beam is converted into electricity by the piezoelectric film.

It is argued in Ref. [10] that in order to scavenge energy efficiently from a variety of vibration sources, an energy scavenger should have sufficient bandwidth in designated frequency intervals. A device with such a property is nothing but a mechanical band-pass filter.

In Ref. [10], a mechanical band-pass filter is proposed. The proposed filter is an ensemble of beam–mass systems; see Fig. 2. It is shown in Ref. [10] that such an ensemble can be made into a band-pass filter when

*Tel.: +1510 526 1666.
E-mail address: shahruz@cal.berkeley.edu.

0022-460X/$ - see front matter © 2005 Elsevier Ltd. All rights reserved.
doi:10.1016/j.jsv.2005.09.022

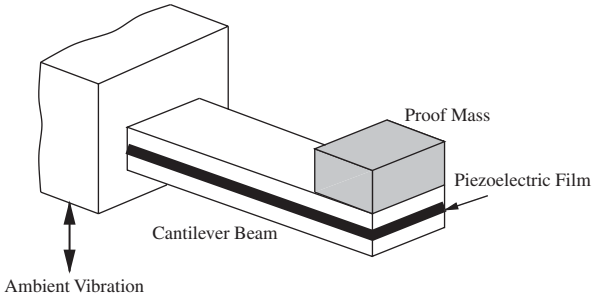

Fig. 1. A typical energy scavenger consists of a cantilever beam on which a piezoelectric film and a mass, known as the proof mass, are mounted.

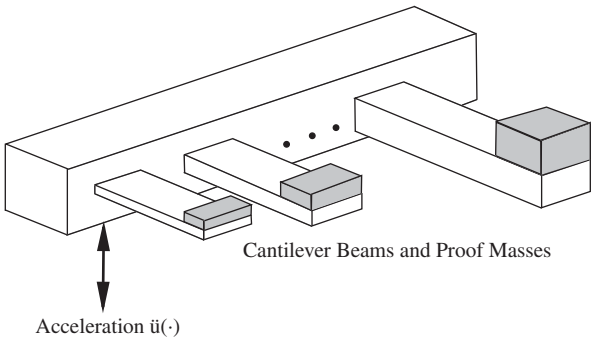

Fig. 2. An ensemble of cantilever beams with proof masses at their tips. When the dimensions of the beams and masses of the proof masses are chosen appropriately, this ensemble can function as a band-pass filter.

dimensions of the beams and masses of the proof masses are chosen appropriately. Moreover, it is shown that the frequency band of the filter is limited and cannot be chosen arbitrarily large: the frequency band is independent of dimensions of the beams and masses of the proof masses.

In this note, the goal is to determine the limits of performance of the device in Fig. 2 when it functions as a band-pass filter. The organization of the note is as follows. In Section 2, a mathematical model that describes the transversal vibration of a beam–mass system is presented. In Section 3, using the results for one beam–mass system, the limits of performance of the device in Fig. 2 are determined. Based on such limits, a systematic procedure for determining dimensions of the beams and masses of the proof masses of high-performance band-pass filters is given. In Section 4, two examples are presented.

2. A mathematical model of vibrating beam–mass systems

In Fig. 3, consider a schematic of the beam–mass system shown in Fig. 1. The length, width, and thickness of the beam are denoted by l, w, and h, respectively. The mass density and the modulus of elasticity of the beam are denoted by ρ and E, respectively. The proof mass at the tip of the beam is assumed to be a point mass of mass M. The vibration source on which the cantilever beam is mounted exerts the acceleration $\ddot{u}(\cdot)$. Due to this external input, the beam vibrates transversally. The transversal displacement of the beam at an $x \in [0, l]$ and a $t \geqslant 0$ is denoted by $y(x, t) \in \mathbb{R}$.

With this setup, a mathematical model describing the dynamics of the beam–mass system is derived in Ref. [10]. This model, which is adopted in this note, is based on the generalized single-degree-of-freedom (sdof) system corresponding to the beam–mass system; see, e.g., Ref. [11, pp. 140–145] for the definition of the generalized sdof system. The model is described briefly in the following. The transversal displacement of the

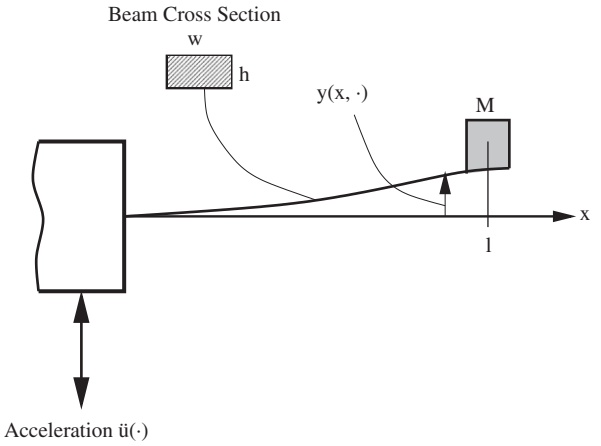

Fig. 3. A schematic of a beam with a proof mass at its tip. The vibration source exerts the acceleration $\ddot{u}(\cdot)$. The transversal displacement of the beam at an $x \in [0, l]$ and a $t \geqslant 0$ is denoted by $y(x, t)$.

beam is written as

$$y(x,t) = \phi(x)q(t), \tag{1}$$

for all $x \in [0, l]$ and $t \geqslant 0$. In Eq. (1), the real- and scalar-valued function $x \mapsto \phi(x)$ is chosen as

$$\phi(x) = a(\alpha)\left(\frac{x}{l}\right)^2 - b(\alpha)\left(\frac{x}{l}\right)^3, \tag{2}$$

for all $x \in [0, l]$, with

$$\alpha := \frac{M}{\rho whl}, \tag{3a}$$

$$a(\alpha) = \frac{\sin\lambda(\alpha) + \sinh\lambda(\alpha)}{\cos\lambda(\alpha) + \cosh\lambda(\alpha)}\lambda^2(\alpha), \quad b(\alpha) = \frac{1}{3}\lambda^3(\alpha), \tag{3b}$$

where the dependence of λ on α is given in Ref. [12, p. 188, Table 6.7(a)].

The real- and scalar-valued function $t \mapsto q(t)$ in Eq. (1) is the solution of following second-order ordinary differential equation:

$$m\ddot{q}(t) + c\dot{q}(t) + kq(t) = -f\ddot{u}(t), \quad q(0) = 0, \quad \dot{q}(0) = 0, \tag{4}$$

for all $t \geqslant 0$, where c is a positive real number known as the damping coefficient, and

$$m := a_1(\alpha)M + a_2(\alpha)\rho whl, \quad k := \frac{a_3(\alpha)Ewh^3}{3l^3}, \quad f := a_4(\alpha)M + a_5(\alpha)\rho whl, \tag{5}$$

with

$$a_1(\alpha) := [a(\alpha) - b(\alpha)]^2, \quad a_2(\alpha) := \frac{a^2(\alpha)}{5} - \frac{2a(\alpha)b(\alpha)}{6} + \frac{b^2(\alpha)}{7}, \tag{6a}$$

$$a_3(\alpha) := a^2(\alpha) - 3a(\alpha)b(\alpha) + 3b^2(\alpha), \tag{6b}$$

$$a_4(\alpha) := a(\alpha) - b(\alpha), \quad a_5(\alpha) := \frac{a(\alpha)}{3} - \frac{b(\alpha)}{4}. \tag{6c}$$

Using the value of α and the corresponding $\lambda(\alpha)$ in Ref. [12, p. 188, Table 6.7(a)], $a(\alpha)$ and $b(\alpha)$ in Eq. (3b) can be computed for all $\alpha \geqslant 0$. Having these quantities computed, it can be verified numerically that $0 < a_i(\alpha) < \infty$ for all $\alpha \geqslant 0$ and $i = 1, 2, \ldots, 5$. The damping ratio corresponding to both system (4) and the beam–mass

system is defined as

$$\xi := \frac{c}{2(mk)^{1/2}}. \tag{7}$$

By applying the Laplace transform to Eq. (1), it follows that

$$y(x,s) = \phi(x)q(s), \tag{8}$$

for all $x \in [0,l]$, where $y(x,s)$ and $q(s)$ are the Laplace transforms of $y(x,\cdot)$ and $q(\cdot)$, respectively. A transfer function, which relates the displacement of the tip of the beam to the applied acceleration, is defined as

$$g_{\text{tip}}(s) := \frac{y(l,s)}{\ddot{u}(s)}, \tag{9}$$

where $\ddot{u}(s)$ is the Laplace transforms of $\ddot{u}(\cdot)$. Using Eqs. (8), (2), (6c), and (4) in Eq. (9), it is concluded that

$$g_{\text{tip}}(s) = \frac{\phi(l)q(s)}{\ddot{u}(s)} = -\frac{a_4 f}{ms^2 + cs + k}. \tag{10}$$

The H_∞-norm of the transfer function $g_{\text{tip}}(s)$ is defined as

$$\|g_{\text{tip}}\|_\infty := \max_{\omega \in \mathbb{R}} |g_{\text{tip}}(\mathrm{j}\omega)|, \tag{11}$$

where $\mathrm{j} = \sqrt{-1}$. The norm $\|g_{\text{tip}}\|_\infty$ corresponds to the global maximum of the Bode magnitude plot of the transfer function $g_{\text{tip}}(s)$. The magnitude $|g_{\text{tip}}(\mathrm{j}\omega)|$ attains its maximum at the resonant frequency denoted by ω_r.

When $0 < \xi \ll 1$, it is shown in Ref. [10] that

$$\omega_r = \left(\frac{a_3(\alpha) E w h^3}{3[a_1(\alpha)M + a_2(\alpha)\rho w h l] l^3} \right)^{1/2}, \tag{12a}$$

$$\|g_{\text{tip}}\|_\infty = \frac{3a_4(\alpha)[a_4(\alpha)M + a_5(\alpha)\rho w h l] l^3}{2\xi a_3(\alpha) E w h^3}, \tag{12b}$$

for all $\alpha \geqslant 0$, where the constant coefficients $a_1(\alpha), a_2(\alpha), \ldots, a_5(\alpha)$ are given in Eq. (6).

The resonant frequency ω_r and the norm $\|g_{\text{tip}}\|_\infty$ are used in the design of mechanical band-pass filters.

3. Limits of performance of the band-pass filter

In this section, the ensemble of beam–mass systems shown in Fig. 2 is considered. The following questions are then raised: (i) What is the best possible performance of the device in Fig. 2 when it functions as a band-pass filter? (ii) How can a device with such a performance be designed? In answering these questions, the limits of performance of the device are determined. Knowledge of such limits leads to a systematic procedure for determining dimensions of the beams and masses of the proof masses that make the device in Fig. 2 into a high-performance band-pass filter.

3.1. Limits of performance

In Ref. [10], in order to have the device in Fig. 2 function as a band-pass filter, dimensions of the beams and masses of the proof masses are chosen such that: (i) resonant frequencies ω_r of the beam–mass systems of the device are different from each other; (ii) norms $\|g_{\text{tip}}\|_\infty$ corresponding to all beam–mass systems assume a same constant value, say $\gamma^* > 0$. Condition (ii) is now replaced by

$$\|g_{\text{tip}}\|_\infty = \gamma(\omega_r), \tag{13}$$

where $\omega_r \mapsto \gamma(\omega_r)$ is a positive and bounded function defined on the domain $D(\gamma) \subset \mathbb{R}_+ \backslash \{0\}$. The domain $D(\gamma)$, which is the frequency band of the filter to be designed, is chosen by the designer. The function $\omega_r \mapsto \gamma(\omega_r)$,

which is the locus of the peaks of the Bode magnitude plots of the transfer functions $g_{\text{tip}}(s)$, is chosen from a class of functions. This class of functions will be characterized in this section.

Clearly, the performance of the device in Fig. 2 depends on the function $\omega_r \mapsto \gamma(\omega_r)$. The question is: What is the class of functions $\omega_r \mapsto \gamma(\omega_r)$ for which the device in Fig. 2 is physically realizable? This class, to be characterized in the following, achieves two useful results: (i) it reveals the limits of performance of the device in Fig. 2 when it functions as a band-pass filter; (ii) it facilitates the design of a variety of physically realizable and high-performance band-pass filters.

Following the steps in Ref. [10], in Eq. (12b), the norm $\|g_{\text{tip}}\|_\infty$ is set equal to $\gamma(\omega_r)$. The result is

$$\gamma(\omega_r) = \frac{3a_4(\alpha)[a_4(\alpha)M + a_5(\alpha)\rho whl]l^3}{2\xi a_3(\alpha)Ewh^3}, \tag{14}$$

for all $\omega_r \in D(\gamma)$. Using Eq. (3a) in Eq. (14), it follows that

$$l^4 = \left(\frac{2a_3(\alpha)E\xi\gamma(\omega_r)}{3a_4(\alpha)[\alpha a_4(\alpha) + a_5(\alpha)]\rho}\right)h^2, \tag{15}$$

for all $\omega_r \in D(\gamma)$. Substituting Eqs. (3a) and (15) into Eq. (12a), it is concluded that

$$\gamma(\omega_r) = H(\alpha)\left(\frac{1}{\xi\omega_r^2}\right), \tag{16}$$

for all $\omega_r \in D(\gamma)$, where

$$H(\alpha) := \frac{a_4(\alpha)[\alpha a_4(\alpha) + a_5(\alpha)]}{2[\alpha a_1(\alpha) + a_2(\alpha)]}, \tag{17}$$

for all $\alpha \geqslant 0$. The scalar-valued function $\alpha \mapsto H(\alpha)$ is evaluated by using the values of α and the corresponding $\lambda(\alpha)$ in Ref. [12, p. 188, Table 6.7(a)] and Eqs. (3b) and (6); results are plotted in Fig. 4. It is evident from this

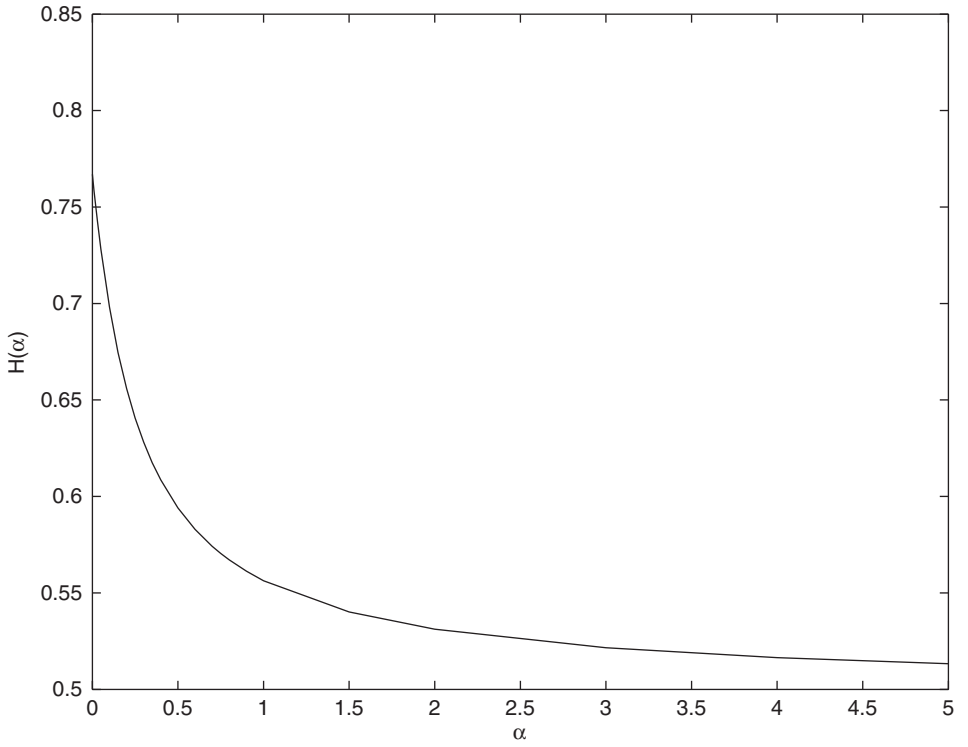

Fig. 4. Graph of the function $\alpha \mapsto H(\alpha)$ in Eq. (17).

figure that $\alpha \mapsto H(\alpha)$ is a monotonically decreasing function of α. Therefore, from Eq. (16), it follows that

$$\frac{0.5}{\xi\omega_r^2} = \frac{a_4^2(\infty)}{2a_1(\infty)}\left(\frac{1}{\xi\omega_r^2}\right) < \gamma(\omega_r) \leqslant \frac{a_4(0)a_5(0)}{2a_2(0)}\left(\frac{1}{\xi\omega_r^2}\right) = \frac{0.767}{\xi\omega_r^2}, \tag{18}$$

for all $\omega_r \in D(\gamma)$. From Eq. (6), it is noted that $a_4^2(\alpha)/a_1(\alpha) = 1$ for all $\alpha \geqslant 0$. This fact establishes the inequality on the left-hand side of inequality (18).

The class of functions $\omega \mapsto \gamma(\omega_r)$ is thus characterized by inequality (18). This class consists of functions the graphs of which lie between those of the following scalar-valued functions:

$$\gamma_l(\omega_r) := \frac{0.5}{\xi\omega_r^2}, \quad \gamma_u(\omega_r) := \frac{0.767}{\xi\omega_r^2}, \tag{19}$$

for all $\omega_r \in D(\gamma)$. Graphs of the functions in Eq. (19) for $\xi = 0.01$ are depicted in Fig. 5. By inequality (18), no part of the graph of $\omega_r \mapsto \gamma(\omega_r)$ can lie above that of $\omega_r \mapsto \gamma_u(\omega_r)$, because such a situation implies that $\alpha < 0$ (equivalently, the proof mass $M < 0$). Neither can a part of the graph of $\omega_r \mapsto \gamma(\omega_r)$ lie on or below that of $\omega_r \mapsto \gamma_l(\omega_r)$, because such a situation implies that α (equivalently, M) is infinitely large.

In Ref. [10], the function $\gamma(\omega_r) = \gamma^* > 0$ for all $\omega_r \in D(\gamma) = (\omega_{\min}, \omega_{\max}]$; see Fig. 6(a). By inequality (18), however, any function $\omega_r \mapsto \gamma(\omega_r)$ the graph of which lies between those of $\omega_r \mapsto \gamma_l(\omega_r)$ and $\omega_r \mapsto \gamma_u(\omega_r)$ can be chosen. For instance, see the graphs in Figs. 6(b) and 6(c).

It is clear that the functions $\omega_r \mapsto \gamma_l(\omega_r)$ and $\omega_r \mapsto \gamma_u(\omega_r)$ determine the limits of performance of the device in Fig. 2 when it functions as a band-pass filter. Within the confines of these functions, $\omega_r \mapsto \gamma(\omega_r)$ should be chosen appropriately in order to make the device in Fig. 2 into a high-performance band-pass filter.

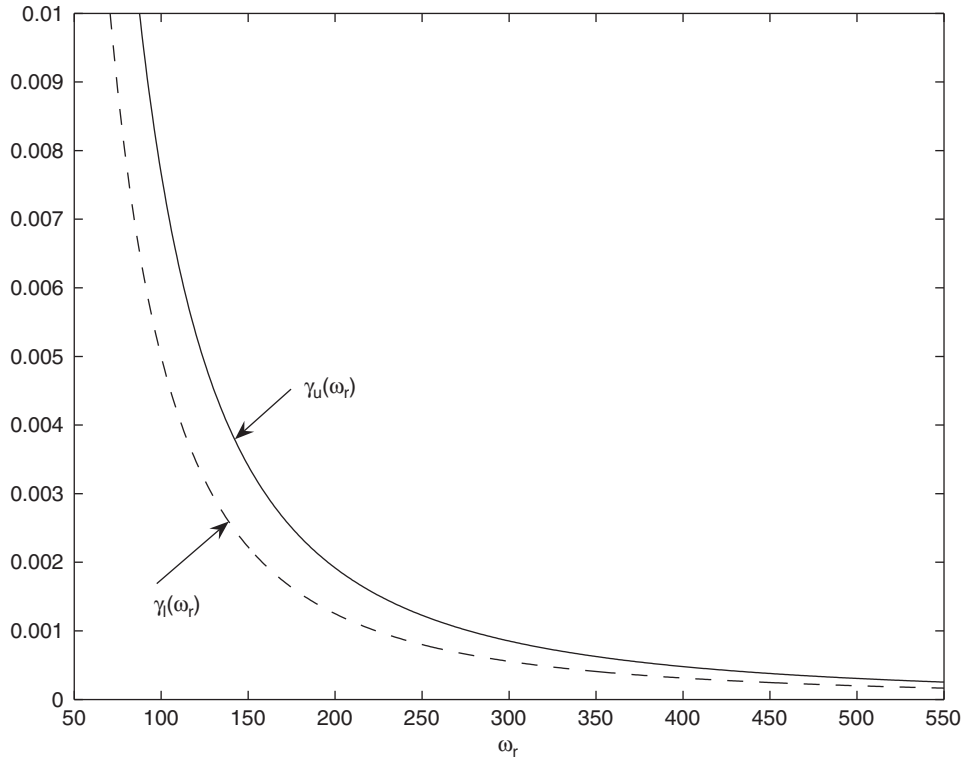

Fig. 5. Graphs of the functions $\omega_r \mapsto \gamma_l(\omega_r)$ and $\omega_r \mapsto \gamma_u(\omega_r)$ in Eq. (19) for $\xi = 0.01$ shown, respectively, by dashed and solid lines. On $\omega_r \mapsto \gamma_u(\omega_r)$, the proof mass $M = 0$, and on $\omega_r \mapsto \gamma_l(\omega_r)$, the proof mass $M = \infty$.

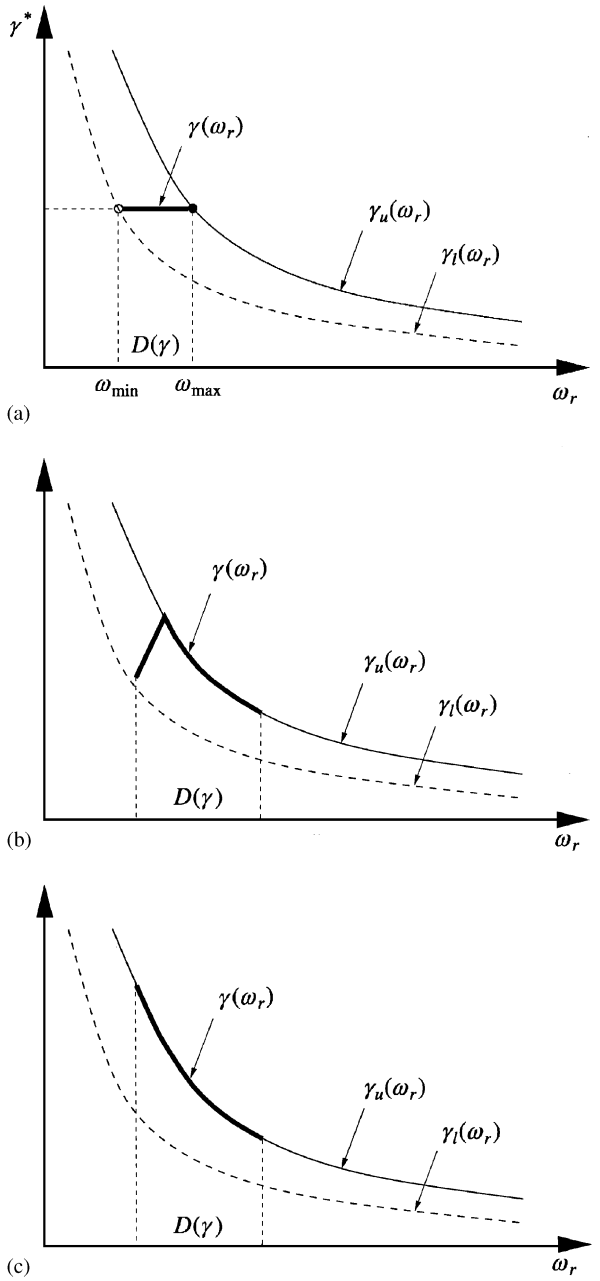

Fig. 6. Different choices of the function $\omega_r \mapsto \gamma(\omega_r)$ shown by thick solid lines: (a) the function assumes the constant value $\gamma^* > 0$; (b) the function first increases and then decreases while its graph lies on that of $\omega_r \mapsto \gamma_u(\omega_r)$; (c) the function decreases while its graph lies on that of $\omega_r \mapsto \gamma_u(\omega_r)$. Graphs of all three functions $\omega_r \mapsto \gamma(\omega_r)$ lie between those of the limiting functions $\omega_r \mapsto \gamma_l(\omega_r)$ and $\omega_r \mapsto \gamma_u(\omega_r)$ shown, respectively, by dashed and solid lines.

3.2. A systematic design procedure

In the following, a systematic procedure is given to determine dimensions of the beams and masses of the proof masses of the device in Fig. 2.

Procedure 3.1. Take the following steps to obtain l, w, and h of the beams and M of the proof masses that make the device in Fig. 2 function as a band-pass filter.

Step 1: Knowing the damping ratio $0<\xi\ll 1$, determine the functions $\omega_r \mapsto \gamma_l(\omega_r)$ and $\omega_r \mapsto \gamma_u(\omega_r)$ from Eq. (19). Choose a frequency interval as the frequency band of the desired filter and denote it by $D(\gamma)$. Choose an appropriate function $\omega_r \mapsto \gamma(\omega_r)$ over $D(\gamma)$, such that its graph lies between those of $\omega_r \mapsto \gamma_l(\omega_r)$ and $\omega_r \mapsto \gamma_u(\omega_r)$.

Step 2: Write Eq. (16) as

$$H(\alpha) = \xi\omega_r^2\gamma(\omega_r), \tag{20}$$

for all $\omega_r \in D(\gamma)$. For several $\omega_r \in D(\gamma)$ compute $H(\alpha)$ in Eq. (20) and use Fig. 4 to determine the corresponding α.

Choose a same thickness h for all beams, and use the resonant frequencies ω_r and the corresponding α to compute lengths l via Eq. (15), which is written as

$$l = \left(\frac{2a_3(\alpha)}{3a_4(\alpha)[\alpha a_4(\alpha)+a_5(\alpha)]}\right)^{1/4}\left(\frac{E\xi\gamma(\omega_r)}{\rho}\right)^{1/4}h^{1/2}. \tag{21}$$

Step 3: Choose a same width w for all beams. Use the chosen w together with h and l from Step 2 to compute masses of the proof masses M from Eq. (3a).

Remark. It is recommended to choose the function $\omega_r \mapsto \gamma(\omega_r)$ such that its graph is situated away from that of $\omega_r \mapsto \gamma_l(\omega_r)$. Such a choice guarantees that α (equivalently, M) is not unnecessarily large. It is noted that if $\alpha>2$, then the beam–mass system has a proof mass much heavier than the beam. Such a beam–mass system is not desirable.

Table 1
Dimensions of beams and masses of proof masses in Example 4.1

Beam	α	Frequency ω_r rad/s (Hz)	l (cm)	w (mm)	h (mm)	M (g)
1	2.00	299.18 (47.62)	3.90	4	0.5	1.64
2	1.00	301.50 (47.98)	4.51	4	0.5	0.95
3	0.50	304.89 (48.52)	5.11	4	0.5	0.54
4	0.25	308.92 (49.17)	5.64	4	0.5	0.30
5	0.15	311.76 (49.62)	5.95	4	0.5	0.19
6	0.10	313.68 (49.92)	6.15	4	0.5	0.13
7	0.05	316.09 (50.31)	6.39	4	0.5	0.07
8	0.00	319.13 (50.79)	6.70	4	0.5	0.00
9	0.00	325.00 (51.73)	6.64	4	0.5	0.00
10	0.00	335.00 (53.32)	6.54	4	0.5	0.00
11	0.00	345.00 (54.91)	6.44	4	0.5	0.00
12	0.00	355.00 (56.50)	6.35	4	0.5	0.00
13	0.00	365.00 (58.09)	6.26	4	0.5	0.00
14	0.00	375.00 (59.68)	6.18	4	0.5	0.00
15	0.00	385.00 (61.27)	6.10	4	0.5	0.00
16	0.00	395.00 (62.87)	6.02	4	0.5	0.00
17	0.00	405.00 (64.46)	5.94	4	0.5	0.00
18	0.00	415.00 (66.05)	5.87	4	0.5	0.00
19	0.00	425.00 (67.64)	5.80	4	0.5	0.00
20	0.00	435.00 (69.23)	5.74	4	0.5	0.00
21	0.00	445.00 (70.82)	5.67	4	0.5	0.00
22	0.00	455.00 (72.42)	5.61	4	0.5	0.00
23	0.00	465.00 (74.01)	5.55	4	0.5	0.00
24	0.00	475.00 (75.60)	5.49	4	0.5	0.00
25	0.00	485.00 (77.19)	5.43	4	0.5	0.00
26	0.00	495.00 (78.78)	5.38	4	0.5	0.00
27	0.00	505.00 (80.37)	5.32	4	0.5	0.00
28	0.00	515.00 (81.96)	5.27	4	0.5	0.00

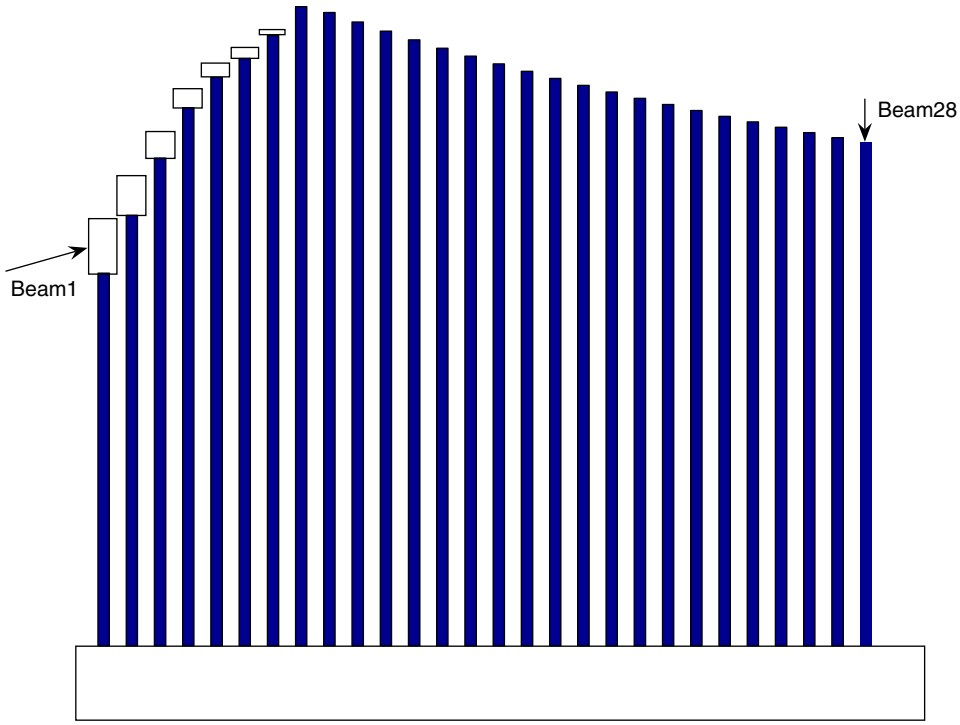

Fig. 7. A realization of the band-pass filter in Example 4.1. Some beams have proofs masses at their tips.

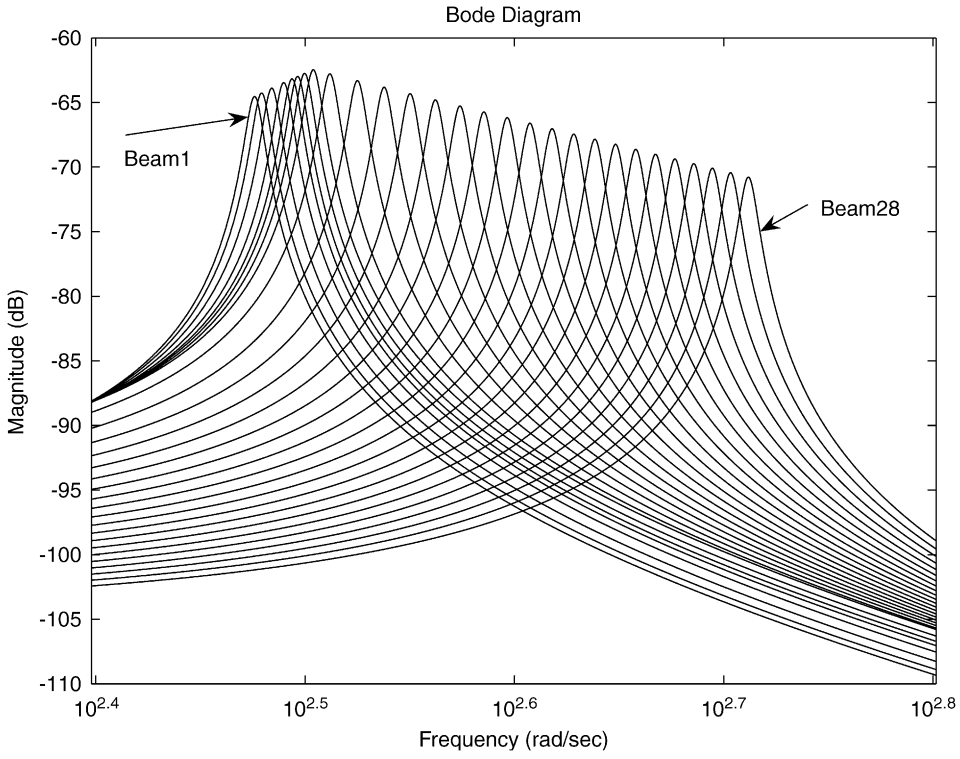

Fig. 8. The Bode magnitude plots of the transfer functions corresponding to the beam–mass systems in Example 4.1.

4. Examples

In this section, two examples are given to illustrate the design of band-pass filters via Procedure 3.1. Suppose that the device in Fig. 2 is to be made out of silver with the following material properties:

$$\rho = 10500\,\mathrm{kg/m^3}, \quad E = 7.8 \times 10^{10}\,\mathrm{N/m^2}, \quad \xi = 0.01. \tag{22}$$

Knowing the damping ratio, the functions $\omega_r \mapsto \gamma_l(\omega_r)$ and $\omega_r \mapsto \gamma_u(\omega_r)$ in Eq. (19) are determined.

Example 4.1. To follow Step 1 of Procedure 3.1, the frequency band of the desired filter is chosen as

$$D(\gamma) = [299.18, 515]\,\mathrm{rad/s} = [47.62, 81.96]\,\mathrm{Hz}. \tag{23}$$

Over $D(\gamma)$, the function $\omega \mapsto \gamma(\omega_r)$ is chosen as

$$\gamma(\omega_r) = \begin{cases} 8 \times 10^{-6}\omega_r - 18 \times 10^{-4}, & \omega_r \in [299.18, 319.13]\,\mathrm{rad/s}, \\ \dfrac{76.70}{\omega_r^2}, & \omega_r \in [319.13, 515]\,\mathrm{rad/s}. \end{cases} \tag{24}$$

It can be easily verified that the graph of $\omega_r \mapsto \gamma(\omega_r)$ lies between those of $\omega_r \mapsto \gamma_l(\omega_r)$ and $\omega_r \mapsto \gamma_u(\omega_r)$. The graph of $\omega_r \mapsto \gamma(\omega_r)$ resembles that shown in Fig. 6(b).

By Step 2 of Procedure 3.1, for several $\omega_r \in D(\gamma)$, the function $H(\alpha)$ in Eq. (20) is computed. Then, for each ω_r, the corresponding α is determined from Fig. 4. Results are listed in Table 1.

Table 2
Dimensions of beams and masses of proof masses in Example 4.2

Beam	Frequency ω_r rad/s (Hz)	l (cm)	w (mm)	h (mm)	M (g)
1	300.00 (47.75)	6.91	4	0.5	0.00
2	306.10 (48.72)	6.84	4	0.5	0.00
3	312.69 (49.77)	6.76	4	0.5	0.00
4	319.62 (50.87)	6.69	4	0.5	0.00
5	326.83 (52.02)	6.62	4	0.5	0.00
6	334.25 (53.20)	6.54	4	0.5	0.00
7	341.86 (54.41)	6.47	4	0.5	0.00
8	349.64 (55.65)	6.40	4	0.5	0.00
9	357.57 (56.91)	6.33	4	0.5	0.00
10	365.63 (58.19)	6.26	4	0.5	0.00
11	373.81 (59.49)	6.19	4	0.5	0.00
12	382.10 (60.81)	6.12	4	0.5	0.00
13	390.50 (62.15)	6.05	4	0.5	0.00
14	399.00 (63.50)	5.99	4	0.5	0.00
15	407.58 (64.87)	5.92	4	0.5	0.00
16	416.26 (66.25)	5.86	4	0.5	0.00
17	425.01 (67.64)	5.80	4	0.5	0.00
18	433.85 (69.05)	5.74	4	0.5	0.00
19	442.75 (70.47)	5.68	4	0.5	0.00
20	451.73 (71.90)	5.63	4	0.5	0.00
21	460.78 (73.33)	5.57	4	0.5	0.00
22	469.89 (74.78)	5.52	4	0.5	0.00
23	479.06 (76.24)	5.47	4	0.5	0.00
24	488.29 (77.71)	5.41	4	0.5	0.00
25	497.58 (79.19)	5.36	4	0.5	0.00
26	506.93 (80.68)	5.31	4	0.5	0.00
27	516.33 (82.18)	5.26	4	0.5	0.00
28	525.78 (83.68)	5.22	4	0.5	0.00

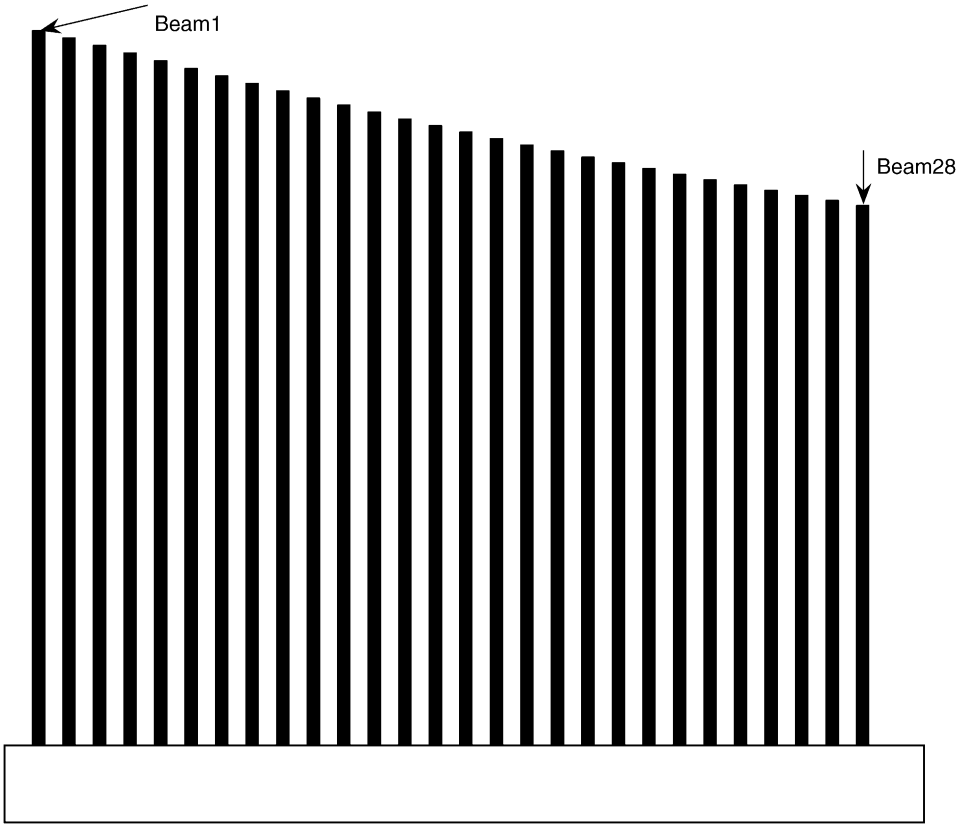

Fig. 9. A realization of the band-pass filter in Example 4.2. No beam has a proof mass at its tip.

The same thickness $h = 0.0005\,\text{m}$ is chosen for all beams. Then, using the resonant frequencies ω_r and the corresponding α, lengths of the beams are computed via Eq. (21). Results are listed in Table 1 as h and l.

The same width $w = 0.004\,\text{m}$ is chosen for all beams. By Step 3 of Procedure 3.1, masses of the proof masses are computed from Eq. (3a); they are tabulated as M in Table 1.

The designed band-pass filter has 28 beam–mass systems. The filter can be fabricated as that shown in Fig. 7. The Bode magnitude plots of the transfer functions $g_{\text{tip}}(s)$ corresponding to the beam–mass systems are shown in Fig. 8.

Example 4.2. Consider a setup the same as that in Example 4.1, except that

$$\gamma(\omega_r) = \frac{76.70}{\omega_r^2}, \quad \omega_r \in [300, 525.78]\,\text{rad/s} = [47.75, 83.68]\,\text{Hz}. \tag{25}$$

Graph of the function $\omega_r \mapsto \gamma(\omega_r)$ lies over that of $\omega_r \mapsto \gamma_u(\omega_r)$ given in Eq. (19). The graph of $\omega_r \mapsto \gamma(\omega_r)$ resembles that shown in Fig. 6(c). With this choice, no beam will have a proof mass at its tip.

By applying Procedure 3.1, dimensions of the beams and masses of the proof masses are obtained; results are tabulated in Table 2.

The designed band-pass filter has 28 beam–mass systems. The filter can be fabricated as that shown in Fig. 9. The Bode magnitude plots of the transfer functions $g_{\text{tip}}(s)$ corresponding to the beam–mass systems are shown in Fig. 10.

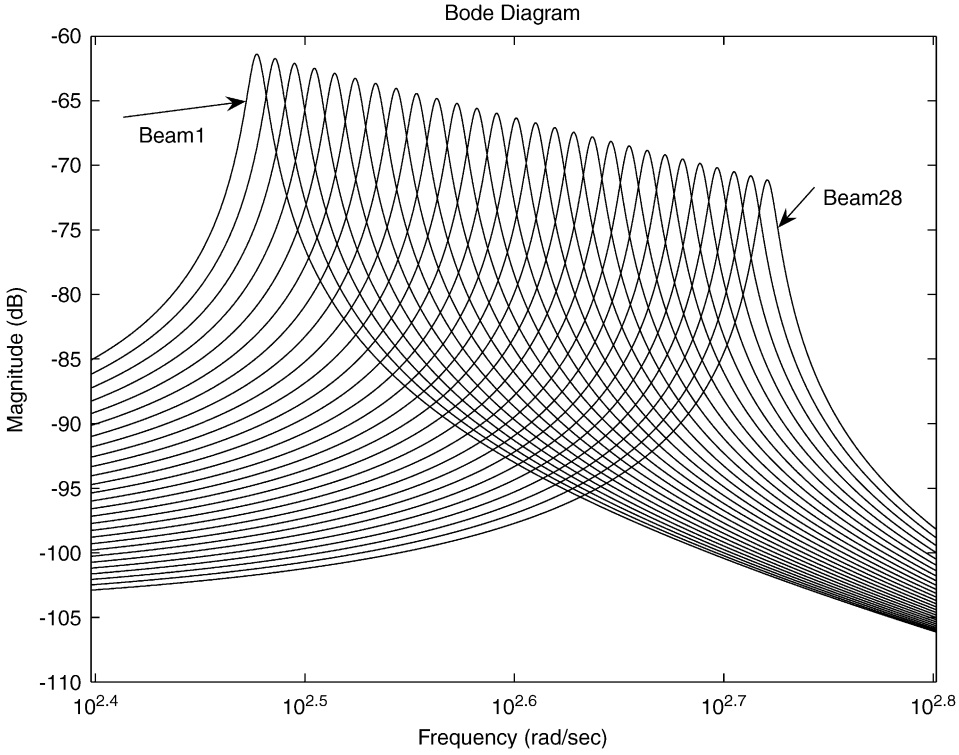

Fig. 10. The Bode magnitude plots of the transfer functions corresponding to the beam–mass systems in Example 4.2.

5. Conclusions

In this note, the limits of performance of mechanical band-pass filters to be used in energy scavenging were obtained. The filter consists of an ensemble of cantilever beams where at the tip of each beam a proof mass is mounted. It was shown that the frequency response of the filter lies between two limiting functions $\omega_r \mapsto \gamma_l(\omega_r)$ and $\omega_r \mapsto \gamma_u(\omega_r)$ in Eq. (19). Knowledge of such limiting functions led to a systematic procedure for determining dimensions of the beams and masses of the proof masses of band-pass filters with best possible performances.

A conclusion of this note, corroborated by Examples 4.1 and 4.2, is that it is advantageous to use the upper limiting function, $\omega_r \mapsto \gamma_u(\omega_r)$, to design band-pass filters. A filter designed using this function has a larger frequency band and there is no need for proof masses at the tips of its cantilever beams; it is thus easily fabricated.

References

[1] C. Shearwood, R.B. Yates, Development of an electromagnetic micro-generator, *Electronics Letters* 33 (22) (1997) 1883–1884.

[2] R. Amirtharajah, A.P. Chandrasakan, Self-powered signal processing using vibration-based power generation, *IEEE Journal of Solid-State Circuits* 33 (5) (1998) 687–695.

[3] S. Meninger, J.O. Mur-Miranda, R. Amirtharajah, A.P. Chandrasakan, J.H. Lang, Vibration-to-electric energy conversion, *IEEE Transactions on Very Large Scale Integration (VLSI) Systems* 9 (1) (2001) 64–76.

[4] N.W. White, P. Glynne-Jones, S.P. Beeby, A novel thick-film piezoelectric micro-generator, *Smart Materials and Structures* 10 (4) (2001) 850–852.

[5] P. Glynne-Jones, S.P. Beeby, N.M. White, Towards a piezoelectric vibration-powered microgenerator, *IEE Proceedings—Science, Measurement and Technology* 148 (2) (2001) 68–72.

[6] P.D. Mitcheson, T.C. Green, E.R. Yeatman, A.S. Holmes, Architectures for vibration-driven micropower generators, *Journal of Microelectromechanical Systems* 13 (3) (2004) 429–440.
[7] Y. Yoshitake, T. Ishibashi, A. Fukushima, Vibration control and electricity generating device using a number of hula-hoops and generators, *Journal of Sound and Vibration* 275 (1–2) (2004) 77–88.
[8] H.A. Sodano, D.J. Inman, G. Park, A review of power harvesting from vibration using piezoelectric materials, *The Shock and Vibration Digest* 36 (3) (2004) 197–205.
[9] S. Roundy, P.K. Wright, J. Rabaey, *Energy Scavenging for Wireless Sensor Networks: With Special Focus on Vibrations*, Kluwer Academic Publishers, Boston, MA, 2004.
[10] S.M. Shahruz, Design of mechanical band-pass filters for energy scavenging, *Journal of Sound and Vibration*, (2005), in press.
[11] R.W. Clough, J. Penzin, *Dynamics of Structures*, second ed., McGraw-Hill, New York, NY, 1993.
[12] I.A. Karnovsky, O.I. Lebed, *Free Vibration of Beams and Frames*, McGraw-Hill, New York, NY, 2004.